Quaternion Joint: Dexterous 3-DOF Joint Representing Quaternion Motion for High-Speed Safe Interaction*

Yong-Jae Kim, Jong-In Kim, and Wooseok Jang

Abstract— This paper presents a dexterous three degree-of-freedom (3-DOF) wrist mechanism with a large range of motion and uniform manipulability without singular points throughout the entire range of motion. It has a 2-DOF spherical pure rolling joint surrounded by two pairs of actuating wires, the motions of which directly represent the quaternion values of the joint; this joint is therefore named the quaternion joint. Based on this property, it has simple and clear forward and inverse kinematics and high manipulability. By adding a 1-DOF rotation joint at the distal end of the quaternion joint, it can be extended to a 3-DOF joint mechanism. To precisely approximate the spherical pure rolling motion in a confined central space, a novel parallel mechanism composed of three identical supporting linkages was introduced. Unlike conventional parallel mechanisms, it has a compact and simple structure with no interference among the supporting linkages. Because the wrist mechanism is a tendon-driven mechanism, and is thus suitable for lightweight manipulators, it is mounted to a low-inertia manipulator with high stiffness and strength, namely, LIMS2-AMBIDEX, which is an improved version of the authors' previous research. The basic concept and thorough theoretical analysis of the wrist mechanism are described herein, and the simulations and experiments conducted for a quantitative validation are presented.

I. INTRODUCTION

The efforts to develop inherently safe and highly performing manipulators have been continuously pursued, and in recent years various cooperative robots have been introduced into the market. Such manipulators are being developed to assist or replace tedious or dangerous work by sharing common workspace and tools safely with humans without too much intervention by experts.

To achieve a proper level of safety, various approaches are being attempted. The first approach was adding precise force or torque sensors to conventional industrial manipulators [1]. This allowed most of the advantages of industrial manipulators to be maintained, such as a high repeatability and payload, as well as safe interactions with humans at a relatively low speed [2]. However, at high speeds, the large mass and inertia of a manipulator can be dangerous to humans because it causes high kinetic and potential energy, and force or torque sensors cannot rapidly diminish an impact. For instance, at a velocity of 6 m/s, which is common in interactions among humans, even a lightweight industrial robot can exceed head injury criteria(HIC) level 1000, which is a life-threatening value [3].
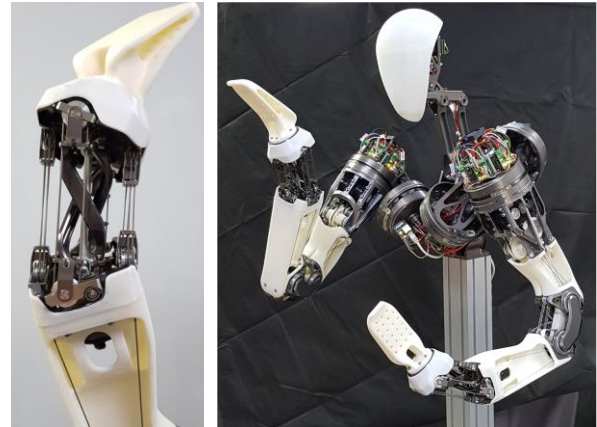

Fig. 1. Developed quaternion joint and low-inertia high-stiffness manipulator, LIMS2-AMBIDEX, using the proposed wrist mechanism.

The addition of a compliant component between the link and actuators to absorb an impact and increase compliance is a promising approach. Various series elastic actuators (SEAs) [4] and variable stiffness joints (VSJs) [5] have been developed and applied to manipulators. Despite their outstanding compliance and safety, they are prone to a relatively low control performance because of limited control bandwidth cause by a low joint stiffness.

The authors believe that lowering the mass and inertia of the manipulator to those of the human arm is one of the ultimate ways to achieve inherent safety. Placing heavy actuators and reduction gears at a proximal part using a tendon-driven mechanism is one of the best ways to achieve a weight minimization [6]. However, a tendon-driven mechanism may have a poor control performance owing to a low stiffness of the tendons. Moreover, increasing the degrees of freedom to seven (7-DOF), similar to a human arm, without increasing the frictional loss or mechanical complexity is very difficult. Thus, in previous research, unique tension amplification mechanisms were applied to a robot with a Low Inertia Manipulator with High Stiffness and Strength (LIMS-AMBIDEX), and demonstrated a high level of performance comparable to industrial robots, as well as safety for humans [3]. Figure 1 shows LIMS2-AMBIDEX that is greatly improved and redevised compared to the LIMS1 especially about the wrist mechanism.

Yong-Jae Kim, is with Korea University of Technology and Education (Koreatech), Cheonan-City, Rep. of Korea (corresponding author to provide phone: +82-41-560-1424; fax: +82-41-564-3261; e-mail: yongjae@koreatech.ac.kr).

Jong-In Kim and Wooseok Jang are with Korea University of Technology and Education (Koreatech), Cheonan-City, Rep. of Korea (e-mail: e4e4my@koreatech. ac.kr, aaeeghj@koreatech.ac.kr).
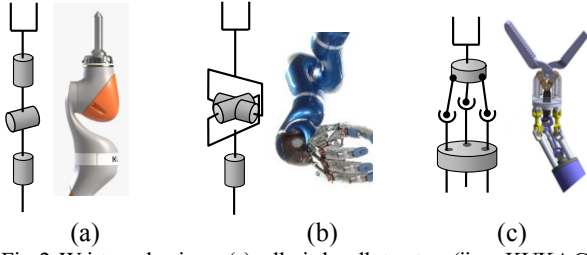
Fig. 2. Wrist mechanisms: (a) roll-pitch-roll structure (iiwa, KUKA Co.), (b) roll-pitch-yaw (Agile Justin, DLR), and (c) parallel mechanism for a surgical instrument (simplified joint structure).
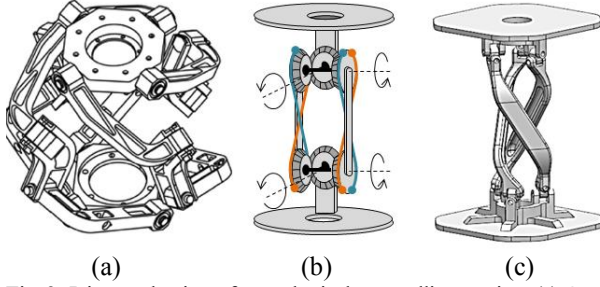

Fig. 3. Joint mechanisms for a spherical pure rolling motion: (a) Omni-wrist III, (b) 2-DOF rolling joint coupled by bevel gears and wires used in LIMS1, and (c) proposed 2-DOF rolling joint using a parallel mechanism.

Most robot wrists used for dexterous manipulation have a 3-DOF mechanism, similar to a human. A wide range of motion and a proper structure to minimize singular poses are highly important factors of the wrist because they are directly related to the performance of the manipulator. However, implementing a compact lightweight wrist mechanism satisfying the aforementioned requirements is a challenge. Figs. 2(a) and 2(b) illustrate conventional robot wrists that are widely used for industrial manipulators [7]. They are relatively simple and reliable, but they are heavy in weight, and have a singular property under certain poses. Although parallel mechanisms, as shown in Fig. 2(c), can reduce the size and weight, and are thus frequently used for surgical instruments [8] or wearable devices [9], they are prone to requiring a complex mechanism, and have difficulty in obtaining a simple kinematic relationship between the actuators and the wrist motion. As introduced in previous research, LIMS1 has a unique wrist structure that utilizes a spherical pure rolling joint, and has a nonsingular property within the entire range of motion. The well-known wrist mechanism, Omni-Wrist III [10], illustrated in Fig. 3(a), is also a spherical pure rolling joint, but is inadequate for tendon actuation because of its large size and link interference. For the wrist of LIMS1, a bevel and wire coupling mechanism as shown in Fig. 3(b) was used to implement a spherical rolling motion; however, this mechanism is complex, and has a low payload and stiffness. In this paper, a new parallel mechanism that approximates a spherical rolling motion and has an extremely simple and compact structure is proposed, as shown in Fig. 3(c). It is notable that the tendon motion is directly proportional to the wrist angle represented by the quaternion notation, and we therefore named the wrist a "quaternion wrist."

The remainder of this paper is organized as follows. Section II reviews the basic concept of the proposed wrist
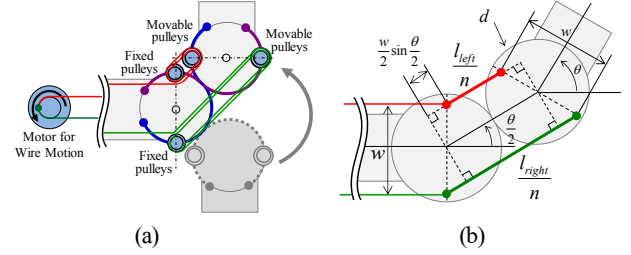

Fig. 4. 1-DOF joint mechanisms with tension amplification mechanisms. (a) basic concept, (b) configuration of actuating wires.
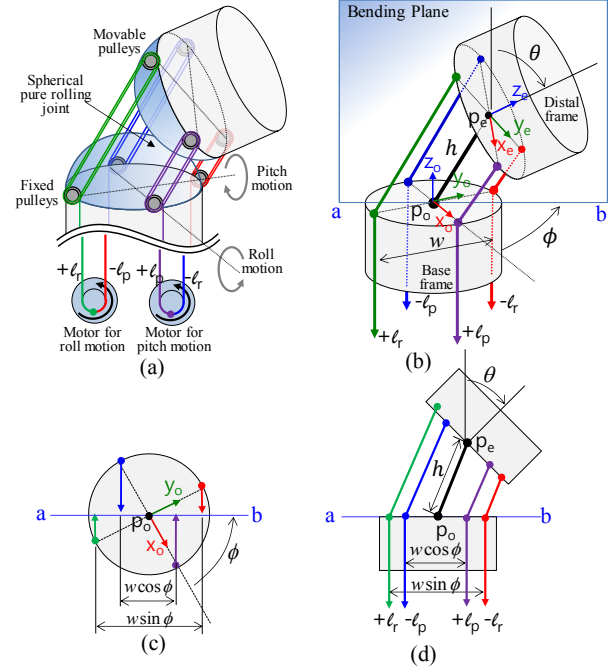

Fig. 5. 2-DOF joint mechanism with spherical rolling joint and tension amplification mechanisms. (a) Basic concept, (b) Bent pose of the mechanism along the bending plane, (c) Top view and (d) side view.

mechanism, which is the same as the previous LIMS1 version. In Section III, the new parallel link mechanism approximating a 2-DOF spherical rolling motion is introduced, and its feasibility and accuracy are described. In Section IV, the kinematic relationship representing the quaternion values is deduced, and a theoretical analysis and comparison of the manipulability with other wrist joints are presented. Section V presents a detailed design and reports the simulation and experimental results, and Section VI provides some concluding remarks.

II. BASIC CONCEPT OF QUATERNION JOINT

In this section, joint mechanisms using the tension amplification mechanisms introduced in [3] are reviewed. Figure 4(a) shows the basic concept of a 1-DOF elbow joint. The joint comprises one circular rolling joint and two actuating wires. The two coupling wires are connected along the circular rolling surface (the blue and purple wires in the figure), enabling a pure rolling motion without slippage. The actuating wires (red and green wires) are placed around the freely rotating fixed and movable pulley sets multiple times, which amplifies the wire tension proportionally to the number of

windings and the wire stiffness in the quadratic order of the winding number. As shown in Fig. 4(b), the displacements of the left and right wires, l_{left} and l_{right}, have the same magnitude but opposite direction, as indicated in the following:

$$l_{left} = -l_{right} = nw\sin\frac{\theta}{2}, \tag{1}$$

where n and w denote the number of wire windings and the distance between the two antagonistic pulley centers. Owing to this symmetric wire motion, the joint can be actuated with a single motor without slack or excessive tension, as shown in the left side of Fig. 4(a). The maximum torque $\tau_{1DOF\ max}$ and the torsional stiffness k_{1DOF} of the 1-DOF joint mechanism are obtained as follows [3]:

$$\tau_{1DOF\ max} = \left(\frac{nw}{2}\cos\frac{\theta}{2}\right)T_{max}, \tag{2}$$

$$\kappa_{1DOF} = \left(\frac{n^2w^2}{2}\cos^2\frac{\theta}{2}\right)k_{wire}, \tag{3}$$

where T_{max} and κ_{wire} indicate the breaking strength and stiffness of the wire. As shown in (3), the stiffness of the wire is amplified n^2 times, which remedies the low stiffness property of the other tendon-driven mechanisms. This advantageous concept can be extended to a 2-DOF joint, as shown in Fig. 5(a). There are two hemispherical rolling surfaces instead of circular-shaped parts, which are surrounded by four actuation wires for the 2-DOF bending motion. The coordinate frame Σ_o, defined using $p_o - x_oy_oz_o$, is attached to the base fame, and Σ_e, defined using $p_e - x_ey_ez_e$, is attached to the distal frame. The displacement of the wire pair (l_r^+, l_r^-) produces a roll motion along the x_O axis, and (l_p^+, l_p^-) produces a pitch motion along the y_O axis. If each wire pair exhibits a symmetrical behavior even under a combined 2-DOF bending motion, this joint also can be actuated using two motors without slack or excessive tension. To prove the symmetricity, let us consider a plane, called a bending plane, where the two centerlines of the base frame and distal frame coexist, as shown in Fig. 5 (b). Here, bending direction ϕ and bending angle θ denote the angle between the x_o axis and the bending plane, and the angle between z_o and z_e on the bending frame, respectively. As shown in the top and side views in Figs. 5(c) and 5(d), the configurations of the two wire pairs are similar to the 1-DOF mechanism, except for the width w between the pulley centers. The equivalent widths for the roll and pitch wire pairs are $w\cos\phi$ and $w\sin\phi$, respectively. Therefore, the relationship between the bending pose (ϕ, θ) and the motion of the wire pair (l_r, l_p) can be obtained as

$$l_r = l_r^+ = -l_r^- = nw\sin\phi\sin\frac{\theta}{2}, \tag{4}$$

$$l_p = l_p^+ = -l_p^- = nw\cos\phi\sin\frac{\theta}{2}, \tag{5}$$

which confirms that the motions of the wire pairs are fully symmetrical. The maximum torque and the torsional stiffness of the 2-DOF joint mechanism are obtained as follows:

$$\tau_{2DOF\ max} = \left(\frac{nw}{2\max(|\cos\phi|,|\sin\phi|)}\cos\frac{\theta}{2}\right)T_{max}, \tag{6}$$

$$\kappa_{2DOF} = \left(\frac{n^2w^2}{2}\cos^2\frac{\theta}{2}\right)k_{wire}. \tag{7}$$

It is notable that the stiffness of the 2-DOF joint is not affected by the bending direction ϕ. This implies that the wrist has the
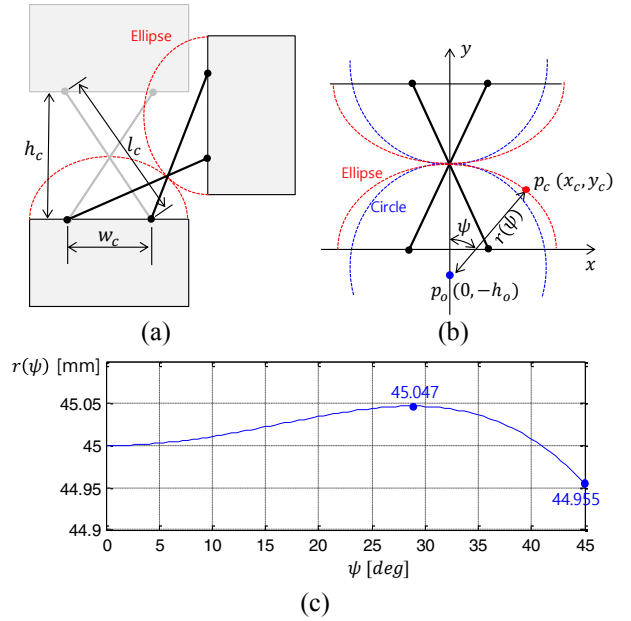

(a) (b)

(c)

Fig. 6. (a) Anti-parallelogram producing a rolling motion along two ellipses, (b) circles approximating the rolling motion, and (c) radius variation of the ellipse.

same stiffness regardless of the bending direction, and is beneficial for a consistent motion control under a particular load. For a detailed explanation, refer to [3].

III. SPHERICAL PURE ROLLING JOINT USING PARALLEL MECHANISM

An anti-parallelogram mechanism can be used to approximate a circular rolling motion. In this section, the conventional anti-parallelogram mechanism approximating a 1-DOF rolling motion is described, and by extending this concept to a 3-dimensional space, a novel parallel mechanism approximating a 2-DOF spherical rolling motion is introduced.

A. Approximation of 1-DOF circular rolling joint

An anti-parallelogram mechanism can produce a pure rolling motion along two ellipses. Figure 5(a) illustrates an anti-parallelogram mechanism and the corresponding ellipses, which are represented by the red curves. By naming the lengths of the short and long links as w_c and l_c, respectively, and the height between the two short links in a straight pose as h_c, the ellipse equation is as follows:

$$\frac{x_c^2}{(l_c/2)^2} + \frac{y_c^2}{(h_c/2)^2} = 1. \tag{8}$$

Let us assume that there is a circle that properly approximates this ellipse, and that its center p_o is placed along the y-axis with offset h_o from the origin, as shown in Fig. 5(b). Considering a line from p_o to a point on the ellipse p_c, the line equation and length of the line r are respectively

$$y_c = \frac{1}{\tan\psi}x_c - h_o, \tag{9}$$

$$r = x_c/\sin\psi, \tag{10}$$

where ψ denotes the angle between the line and the y-axis. By solving x_c using (8) and (9), and substituting it with (10), the length r can be represented as a function of ψ as follows:
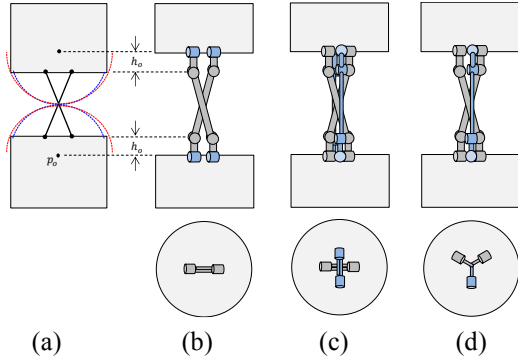
Fig. 7. Basic idea of extending the rolling joint using anti-parallelogram to two dimensions.
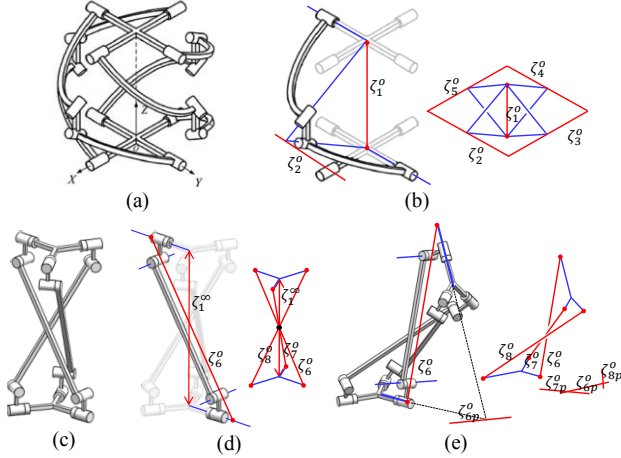

Fig. 8. (a), (b) Kinematic model and constraint wrenches of Omni-Wrist III, and (c), (d), and (e) kinematic model and constraint wrenches of the proposed mechanism.

$$r(\psi) = \frac{h_o + \sqrt{h_o{}^2 + \left(1 + \left(\frac{w_C}{h_C}\right)^2 \tan^2 \psi\right)\left(\left(\frac{w_C}{2}\right)^2 - h_o{}^2\right)}}{\cos\psi\left(1 + \left(\frac{w_C}{h_C}\right)^2 \tan^2 \psi\right)}. \quad (11)$$

If the value remains a near constant, it can be considered that it can approximate the rolling motion between two circles. For instance, if we set w_c, l_c, and h_o as 30, 85.75, and 4.84 mm, respectively, which are similar values as the implemented wrist joint, $r(\psi)$ has an approximately constant value of 45 mm within the error range of 0.05 mm, as shown in Fig. 5(c). It is notable that, if we properly choose the design parameters, the anti-parallelogram can replace the circular rolling joint with reasonable accuracy.

B. Approximation of 2-DOF spherical rolling joint

Figure 7 illustrates the basic idea of extending the rolling joint to 2 DOF using multiple anti-parallelograms. As shown in Fig. 7(b), if revolute joints (blue joints) are added at the end of each link with offset h_o, the mechanism can move freely according to another rolling motion orthogonal to the original 1-DOF rolling direction. Thus, by combining two identical mechanisms perpendicularly to each other, as in Fig. 7(c), a 2-DOF-rolling joint can be implemented. However, this mechanism with four limbs may be redundant or over-constrained. Therefore, when removing one of the limbs and evenly placing the other three limbs, the mechanism can be simplified, as shown in Fig. 7(d). The shapes of middle links

are designed to have an offset, as shown in Figs. 3(c) and 8(c), in order to prevent interference and secure a large hollow space at the center. This 2-DOF spherical rolling mechanism is based on approximated anti-parallelograms. Therefore, it should be verified whether it still has a 2-DOF characteristic without an over-constraint, and whether it can approximate an ideal spherical rolling motion with acceptable accuracy.

C. Mobility Analysis

To examine the mobility or DOF of a mechanism, the Gruebler–Kutzbach criterion (G–K criterion) or modified G-K criteria can traditionally be used. However, they seem unsuitable for an analysis of parallel mechanisms. Thus, a graphical method using reciprocal screw system theory can be applied [11]. For instance, Figs. 8(a) and 8(b) illustrate the kinematic model of Omni-Wrist III and its structure with one of the four limbs highlighted. On the left side of Fig. 8(b), the blue lines represent the rotational freedom line (twist) caused by the revolute joint, and the red lines ζ_1^o and ζ_2^o represent the reciprocal constraint force lines (constraint wrenches), which implies that, along with these constraint directions, translational motions are not allowed. Roughly speaking, these reciprocal force lines can be obtained by finding the lines that intersect all of the rotational freedom lines or are parallel to them. Each limb has two reciprocal force lines and constrains the 2-DOF motion. By combining those of four limbs, as shown on the right side of Fig. (b), the reciprocal force lines form one vertical line ζ_1^o and one rectangular shape on a plane through ζ_2^o, ζ_3^o, ζ_4^o, and ζ_5^o, which restrict the 1- and 3-DOF motions, respectively. Therefore, the remaining DOF of this mechanism is 2. For further information, refer to [11].

The proposed mechanism can be interpreted similarly. Figure 8(d) shows the mechanism under a straight pose, where the rotational freedom lines and constraint lines are presented through the blue and red lines, respectively. As shown on the right side of Fig. 8(d), there are a total of four reciprocal constraint lines, three reciprocal constraint force lines (red lines, ζ_6^o, ζ_7^o, and ζ_8^o), and one constraint torque line (the red line with arrows, ζ_1^∞). The three force lines intersect at one point, and thus restrict the translation in a three-dimensional space, and the torque line restricts the rotation along this line. Therefore, under a straight pose, the remaining DOF is 2. On the other hand, under a bent pose, as indicated in Fig. 8(e), there are a total of six constraint force lines. Here, ζ_{6p}^o, ζ_{7p}^o, and ζ_{8p}^o form a plane constraining the 3 DOFs. It is important that ζ_6^o, ζ_7^o, and ζ_8^o do not intersect the others even when they pass by very closely. This means that, in a strict sense, the proposed mechanism has no mobility under a bent pose. However, if the distance errors among ζ_6^o, ζ_7^o, and ζ_8^o are acceptably small, and it can therefore be considered that they approximately intersect at a single point, ζ_6^o, ζ_7^o, and ζ_8^o only restrict the translational motion. In addition, ζ_{6p}^o, ζ_{7p}^o, and ζ_{8p}^o restrict the 1-DOF rotation along the plane they form. Thus, a 2-DOF motion can be achieved. It is therefore necessary to examine whether the proposed mechanism can have acceptably small assembling errors at the pivots at arbitrary bending direction and bending angle in the entire range of motion.

C. Assembly and Approximation Errors

To obtain the assembly errors under a certain bent pose, a constrained optimization is applied. As shown in Fig. 9(a), the
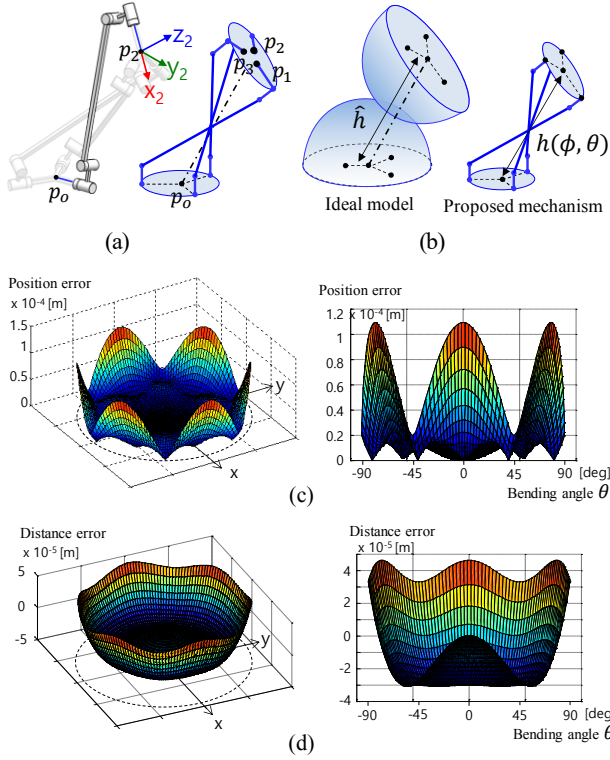
Fig. 9. (a) and (b) Joint configuration at the bent pose, (c) and (d) position and distance errors between the ideal model and proposed mechanism.

three limbs are regarded as individual open-chain manipulators, and the end-effector frames and points are defined as Σ_1, Σ_2, and Σ_3, and as p_1, p_2, and p_3, respectively. Assuming that the desired bending direction ϕ and bending angle θ are given, the optimization objective is as follows:

$$\min \frac{1}{3}\sum_{i\neq j}\|p_i p_j\|, \quad \text{subject to:} \ z_i = z_d \ \text{for} \ \forall i \quad (12)$$

where z_d and z_i denote a unit vector to the z-axes of the desired rotation matrix calculated from ϕ and θ and that of the z-axis of ith limb's end-effector orientation. This determines the minimum value of the average distance error of the end-effector positions of the three open-chain limbs while satisfying the desired bending direction and angle. The design parameters w_c, l_c, and h_o were set to 30, 85.25, and 5.1 mm, respectively, which were chosen to approximate the spherical rolling motion with 90 mm diameter spheres. The range of motion was $\phi = [-\pi, \pi)$ and $\theta = [0, \pi/2)$. Figure 9(c) shows the obtained average distance error within the entire range of motion. The error is zero under a straight pose ($\theta = 0$, at the center of the graph), and the maximum error is 0.109 mm under fully bent poses ($\theta = \pi/2$ and $\phi = \frac{n\pi}{3}$, where $n = 0, \cdots, 5$). This value can be considered reasonably small, and can be absorbed in the mechanical tolerance of the pivots and links of the mechanism. Similarly, how well it approximates the spherical rolling motion can be examined. Figure 9(b) shows the difference in diameter of the rolling surface between the ideal and actual models, where the ideal model has a constant diameter of $\hat{h} = 90$ mm, whereas the actual mechanism has the function of the bending direction and bending angle $h(\phi, \theta)$. The error, $\hat{h} - h(\phi, \theta)$, is as shown in Fig. 9(c). The maximum error is 0.0046 mm, which

is an acceptably small value. Note that these distance and diameter errors are repeated every 60° of the bending direction because the mechanism has the same limb structures every 120°, and has plane symmetry every 60°.

Consequently, the proposed 2-DOF rolling joint can approximate an ideal spherical rolling motion with high accuracy with an error of 0.0046 mm. Unlike other spherical rolling mechanisms, it has a compact and simple structure, which is highly suitable for tendon driven actuation, as shown in Fig. 5(a). Moreover, because the links have straight shapes and their connected pose is almost straight (when comparing the shapes in Figs. 8(b) and 8(d)), they can endure a high load with a thin structure.

IV. KINEMATICS AND MANIPULABILITY

In this section, the kinematic relationship between an actuating wire movement and a bending motion is investigated. As illustrated in Fig. 5(b), the base frame Σ_o and the moving frame Σ_b are placed at points p_o and p_e, respectively. Considering the bending direction ϕ and bending angle θ, the homogeneous transform from Σ_o to Σ_e is as follows:

$$^oT_e = R_z(\phi)R_y\left(\frac{\theta}{2}\right)T_z(h)R_y\left(\frac{\theta}{2}\right)R_z(-\phi)$$

$$= \begin{bmatrix} 1-2\,C^2(\phi)\,S^2\left(\frac{\theta}{2}\right) & -2\,S(2\phi)\,S^2\left(\frac{\theta}{2}\right) & C(\phi)\,S(\theta) & h\,C(\phi)\,S\left(\frac{\theta}{2}\right) \\ -2\,S(2\phi)\,S^2\left(\frac{\theta}{2}\right) & 1-2\,S^2(\phi)\,S^2\left(\frac{\theta}{2}\right) & S(\phi)\,S(\theta) & h\,S(\phi)\,S\left(\frac{\theta}{2}\right) \\ -cC(\phi)\,S(\theta) & -S(\phi)\,S(\theta) & C(\theta) & h\,C(\theta) \\ 0 & 0 & 0 & 1 \end{bmatrix} \quad (13)$$

where $S()$ and $C()$ are a simplified expression of the sine and cosine functions, and h denotes the distance between p_o and p_e, which also means the diameter of the rolling sphere. In addition, R_z, R_y, and T_z indicate the homogeneous transform functions of the z-axis rotation, y-axis rotation, and z-axis translation, respectively. For the ease of representation, the wire displacements l_r and l_p can be scaled using $1/(nw)$. From (4) and (5), the scaled displacements of the roll and pitch wire motions r and p are

$$r \equiv \frac{l_r}{nw} = \sin\phi \sin\frac{\theta}{2}, \quad (14)$$

$$p \equiv \frac{l_p}{nw} = \cos\phi \sin\frac{\theta}{2}. \quad (15)$$

By removing the sinusoidal functions in (13) using (14) and (15), ^oT_e can be rearranged as follows:

$$^oT_e = \begin{bmatrix} 1-2p^2 & 2pr & 2p\eta & hp \\ 2pr & 1-2r^2 & -2r\eta & hr \\ -2p\eta & 2r\eta & 2\eta^2-1 & h\eta \\ 0 & 0 & 0 & 1 \end{bmatrix}, \quad (16)$$

where $\eta^2 = 1 - p^2 - r^2$. Compared to traditional notations such as Euler angles, a quaternion representation has many advantages; for example, it can represent the rotational motion more efficiently, and it does not incur a gimbal lock problem. In general, a rotation matrix and the unit quaternion have the following relationship.

$$\eta_Q = \frac{1}{2}\sqrt{r_{11}+r_{22}+r_{33}+1}$$

$$\epsilon_Q = \frac{1}{2}\begin{bmatrix} \text{sgn}(r_{32}-r_{23})\sqrt{r_{11}-r_{22}-r_{33}+1} \\ \text{sgn}(r_{13}-r_{31})\sqrt{r_{22}-r_{33}-r_{11}+1} \\ \text{sgn}(r_{21}-r_{12})\sqrt{r_{33}-r_{11}-r_{22}+1} \end{bmatrix}, \quad (17)$$
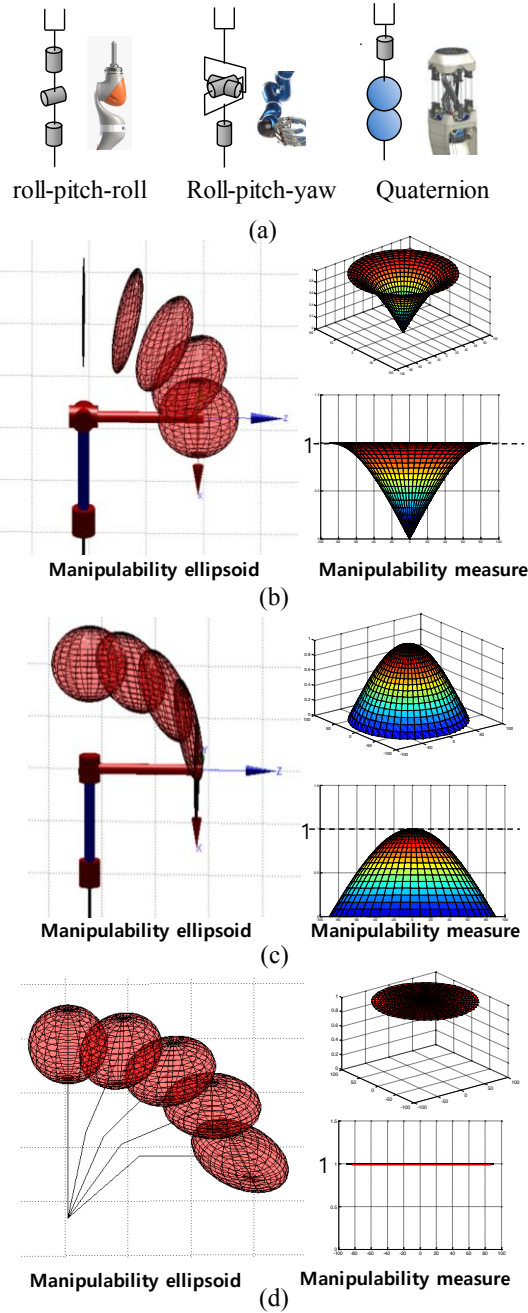
Fig. 10. (a) Three types of wrists in comparison, and (b), (c), and (d) the manipulability ellipsoids and manipulability measure of each type.

where r_{ij} denotes the element of the rotational matrix in the ith row and jth column. Using (16) and (17), the motion of the proposed joint can be represented through a unit quaternion as follows:

$$\eta_Q = \frac{1}{2}\sqrt{(1-2p^2)+(1-2r^2)+(2\eta^2-1)+1} = \eta,$$

$$\epsilon_Q = \frac{1}{2}\begin{bmatrix} sgn(r)\sqrt{(1-2p^2)-(1-2r^2)-(2\eta^2-1)+1} \\ sgn(p)\sqrt{(1-2r^2)-(2\eta^2-1)-(1-2p^2)+1} \\ \sqrt{(2\eta^2-1)-(1-2p^2)-(1-2r^2)+1} \end{bmatrix} = \begin{bmatrix} r \\ p \\ 0 \end{bmatrix}. \quad (18)$$

Therefore, the relationship between the wire motion and the quaternion representation is simply as follows:

$$q_Q = <\eta_Q, \epsilon_Q> = <\eta, r, p, 0>. \quad (19)$$

This means that the scaled wire motions r and p directly correspond to the elements of the quaternion. Thus, the proposed joint is called a quaternion joint. This is significant because it has not only a simplicity of representation but also inherits all mathematical advantages of a quaternion, and can be implemented in a physical space. The differential kinematics can also be obtained using this property. Rewriting (19) using three unit vectors as $q_Q = \eta + r\hat{i} + p\hat{j} + 0\hat{k}$, the angular velocity can be calculated as follows:

$${}^o\omega_e = 2\dot{q}_Q q_Q^* = 2(\dot{\eta} + \dot{r}\hat{i} + \dot{p}\hat{j})(\eta - r\hat{i} - p\hat{j}). \quad (20)$$

By solving this,

$${}^o\omega_e = 2\begin{bmatrix} \dot{r}\eta - r\dot{\eta} \\ \dot{p}\eta - p\dot{\eta} \\ r\dot{p} - \dot{r}p \end{bmatrix} = \begin{bmatrix} \frac{2-2p^2}{\eta} & \frac{2rp}{\eta} \\ \frac{2rp}{\eta} & \frac{2-2r^2}{\eta} \\ -2p & 2r \end{bmatrix}\begin{bmatrix} \dot{r} \\ \dot{p} \end{bmatrix}. \quad (21)$$

Up to this point, a 2-DOF quaternion joint was considered. As described in the previous research, and as shown in Fig. 11(a), a revolute joint for yaw motion can be added at the distal end and form a 3-DOF joint. Let us assign the third frame Σ_t, which is placed at the same position of Σ_e but is rotated along z-axis at angle θ_y. Similar to the wire motions, θ_y can be scaled as $y = \theta_y/(2n_y)$, where n_y is the reduction ratio from the motor to the joint angle. The angular velocity of the 3-DOF quaternion joint can be calculated as follows:

$${}^o\omega_t = {}^o\omega_e + {}^o\omega_{e,t}$$

$$= \begin{bmatrix} \frac{2-2p^2}{\eta} & \frac{2rp}{\eta} \\ \frac{2rp}{\eta} & \frac{2-2r^2}{\eta} \\ -2p & 2r \end{bmatrix}\begin{bmatrix} \dot{r} \\ \dot{p} \end{bmatrix} + {}^oR_e\begin{bmatrix} 0 \\ 0 \\ n_y\dot{\theta}_y \end{bmatrix}$$

$$= \begin{bmatrix} \frac{2-2p^2}{\eta} & \frac{2rp}{\eta} & 4p\eta \\ \frac{2rp}{\eta} & \frac{2-2r^2}{\eta} & -4r\eta \\ -2p & 2r & 4\eta^2-2 \end{bmatrix}\begin{bmatrix} \dot{r} \\ \dot{p} \\ \dot{y} \end{bmatrix} = J_o\dot{q} \quad (22)$$

where ${}^o\omega_{e,t}$ denotes the angular velocity of Σ_t with respect to Σ_e observed in Σ_o, and ${}^oR_e$ indicates the rotation matrix of Σ_e with respect to Σ_t, which can be obtained from (16). In addition, J_o indicates a Jacobian matrix relating the actuation speed and the angular velocity. By differentiating the fourth column of (16), the translational velocity can also be calculated. Therefore, the resultant Jacobian is calculated as follows:

$$\begin{bmatrix} \dot{x} \\ \dot{y} \\ \dot{z} \\ \omega_x \\ \omega_y \\ \omega_z \end{bmatrix} = \begin{bmatrix} 0 & h & 0 \\ h & 0 & 0 \\ -\frac{hr}{\eta} & -\frac{hp}{\eta} & 0 \\ \frac{2-2p^2}{\eta} & \frac{2rp}{\eta} & 4p\eta \\ \frac{2rp}{\eta} & \frac{2-2r^2}{\eta} & -4r\eta \\ -2p & 2r & 4\eta^2-2 \end{bmatrix}\begin{bmatrix} \dot{r} \\ \dot{p} \\ \dot{y} \end{bmatrix} \quad (23)$$

To compare the manipulability of the quaternion joint with other conventional 3-DOF wrists, manipulability ellipsoids and manipulability measures are calculated. Figure 10(a) shows a comparison of the three wrist mechanisms, and Figs.
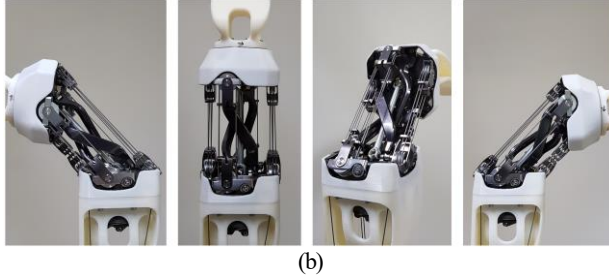
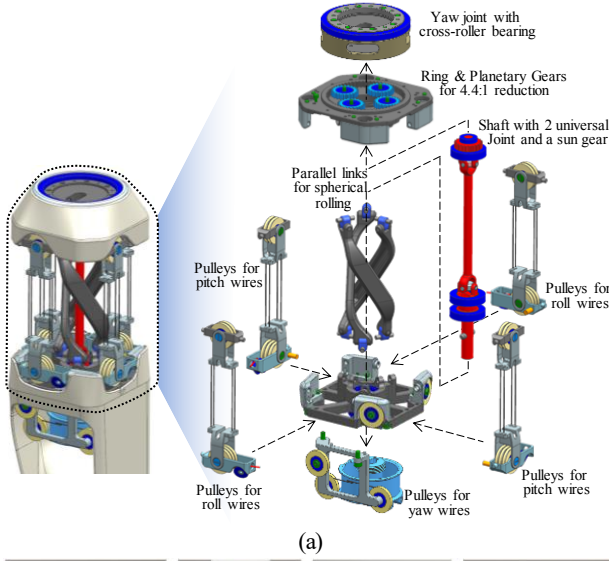| Items	Specifications	
Size and shape	7 DOF per arm - Shoulder 3 DOF, elbow 1 DOF, wrist 3 DOF	
Mass	Arm moving part 2.63 kg - Wrist : 446 g, Forearm : 171 g, Elbow : 533 g - Upper arm (with wrist & elbow motors) :1,478 g Shoulder : 4.17 kg	
Speed	Shoulder roll, pitch :	499 deg/s
	Shoulder Yaw :	749 deg/s
	Elbow :	590 deg/s
	Wrist roll, pitch :	1,179 deg/s
	Wrist yaw :	1,634 deg/s
Peak Torque	Shoulder roll, pitch :	82.0 Nm
	Shoulder Yaw :	54.6 Nm
	Elbow :	69.4 Nm
	Wrist roll, pitch :	34.7 Nm
	Wrist yaw :	25.0 Nm

Fig. 11. (a) Detailed design of the 3-DOF wrist and its exploded view, and (b) implemented wrist joint, with $(\phi, \theta) = (-\pi/2, \pi/2)$, $(0, 0)$, $(\pi, \pi/2)$, and $(\pi/2, \pi/2)$.

10(b)–10(d) show the corresponding manipulability ellipsoids and manipulability measures. Here, the manipulability measures were calculated over the entire range of the first and second joints, and the maximum values were normalized to 1 for a convenience of comparison. The wrist on the left side of Fig. 10(a) is widely applied to industrial manipulators owing to the simple and reliable mechanical structure and the wide range of motion of the distal rotation joint, but has a singular point under a straight pose. As shown in Fig. 10(b), the manipulability ellipsoid has zero volume under a straight pose. The wrist shown in the center of Fig. 10(a) is frequently used for anthropomorphic robots because of its human-like configuration. As shown in Fig. 10(c), it also has a singular pose when it bends at 90°. However, the proposed quaternion wrist shown on the right side of Fig. 10(a) has the same volume of manipulability ellipsoids within the entire range of motion. Moreover, the shapes of the ellipsoids are not too distorted from a sphere, which means that the actuation speed or force is not severely amplified or attenuated within the entire range of motion. It is an advantageous property for motion control owing to the quaternion relationship.

V. Implementation and Experimental Validation

A. Detailed Design and Implementation

Figure 11(a) illustrates the detailed design and an exploded view of the 3-DOF quaternion joint for the LIMS2-AMBIDEX wrist. The parallel links connect the base frame and the distal frame, causing a spherical rolling motion between the two frames. The four pulley sets for the tension amplification of

the roll and pitch wire pairs are attached around the two frames. Because the wires wrap around the pulley sets four times, the tension is amplified 4-fold. By utilizing the hollow space at the center, the distal yaw joint can be actuated. The shaft with two universal joints marked in red transfers the rotation motion to the distal end of the wrist. A sun gear is attached at the top of the shaft, and one ring gear and four planetary gears are included in the distal frame. These form a planetary gear set and provide an additional 4.4:1 reduction for the yaw joint. The three motors for the wrist actuation are placed at the shoulder, and steel wires with diameters of 0.762 mm were used for transmitting the motor motion to the wrist. To minimize the frictional loss, a total of nine pulleys including the pulleys for tension amplification, as shown in Fig. 11(a), are used for the routing of the wires. Therefore, the friction torque of the roll, pitch, and yaw motion is smaller than 1 Nm, and thus a precise measurement of the joint torque by measuring the motor current is possible without the need for expensive torque or force sensors.

Figure 11(b) shows the implemented quaternion wrist. The wrist can bend to ±90 degree in any direction, and the distal yaw joint can rotate 670°. Although the basic concept of the elbows and shoulder is similar to that of the previous version, the performance has been significantly improved. The specifications are briefly summarized in Table I. Please note that the weight of the wrist is only 446 g, which enables safe interaction at high speeds. In addition, the wrist speed exceeds 1,000 degrees/s because the high-power motors used. But its heavy weight does not affect the safety when high-speed motion because they are placed at the proximal part.

B. Verification by Simulations and Experiments

To verify the effectiveness of the quaternion joint, rotating motions were simulated. The bending angle θ was fixed, and the bending direction ϕ was continuously increased to make the end-effector follow a complete circular trajectory with a speed of 1 turn/s. Figure 12(a) indicates the displacements of the scaled roll and pitch wires for two cases. The red and blue solid lines represent a trajectory of $\theta = 90°$, and the dashed lines represent a trajectory of $\theta = 45°$. Figure 12(b) shows the corresponding wire speeds. As these results indicate, the wire displacement and speed are properly regulated without peaks
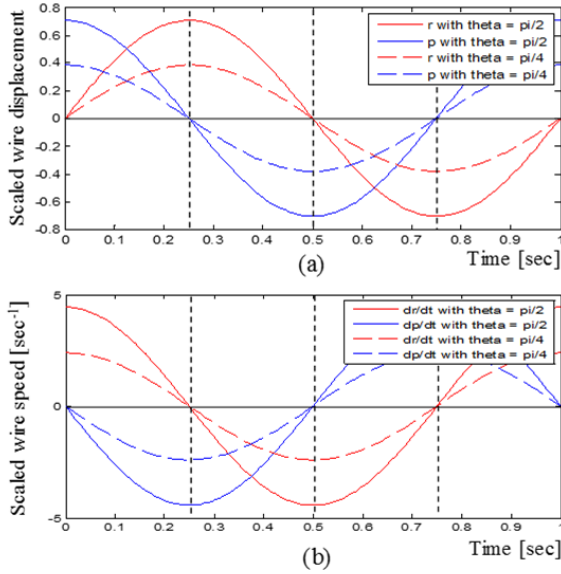
Fig. 12. Displacement and speed of the scaled wires for rotational motion of the quaternion wrist.

(a)

(b)

Fig. 13. (a) Snapshots of load test, and (b) measured and desired wire tensions

thanks to the nonsingular property of the quaternion representation.

To verify the performance of the external load measurement by using motor current, a load test for the wrist was performed. the As shown in Fig. 13(a), a 1 kg load was attached to the end-effector 47 mm from p_e and followed a circular motion of $\theta = 60°$. To satisfy a quasi-static condition, the speed was set to be slow to achieve 1 circle during a period of 20 s. The blue and green curves in Fig. 13(b) represent the measured wire tensions obtained by the motor current, where the coulomb frictions were compensated. The red and black curves show the desired wire tensions. The torque caused by the 1kg load is 0.92Nm and the corresponding maximum tension is 13.37 N, which is a small value to sense using the motor current. However, as the developed mechanism has the low frictional loss, it could efficiently sense the external load.

VI. CONCLUSION AND FUTURE WORK

This paper presented a dexterous 3-DOF wrist mechanism, called a quaternion joint, which has a large range of motion and uniform manipulability without singular points throughout the entire range of motion. It is a wire-driven mechanism, and the motion of the wires directly represents the quaternion motion of the joint. To realize a spherical pure rolling motion in a confined central space, a unique parallel link mechanism was introduced. The simple and reliable structure of this parallel mechanism enables a fast and high payload actuation with a small size and lightness in weight. The weight is 446 g, and the peak torque and speed of the roll and pitch motions are 1,179°/s and 34.7 Nm, respectively.

As future research, control algorithms for a high-speed human-robot interaction achieved by fully utilizing the advantages of LIMS2-AMBIDEX will be investigated. The development of lightweight and dexterous hands for the robot is another important goal.
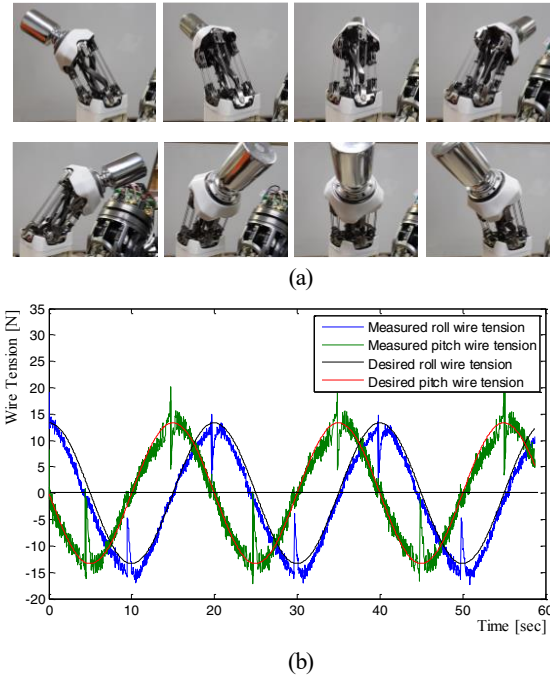
REFERENCES

[1] R. Bischoff et al., "The KUKA-DLR lightweight robot arm—A new reference platform for robotics research and manufacturing," in *Proc. 6th Ger. Conf. Robot.* , pp. 1–8, Jun. 2010.

[2] S. Haddadin, A. Albu-Sch¨affer, and G. Hirzinger, "Requirements for safe robots: Measurements, analysis and new insights," *Int. J. Robot. Res.,* vol. 28, no. 11, pp. 1507–1527, Nov. 2009.

[3] Yong-Jae Kim, "Anthropomorphic Low-Inertia High-Stiffness Manipulator for High-Speed Safe Interaction," *IEEE Transactions on Robotics*, Vol 33, Issue 6, August, 2017.

[4] A. Bicchi and G. Tonietti, "Fast and soft-arm tactics," *IEEE Robot. Autom. Mag.*, vol. 11, no. 2, pp. 22–33, Jun. 2004.

[5] F. Petit, W. et al., "Analysis and synthesis of the bidirectional, antagonistic variable stiffness mechanism," *IEEE/ASME Trans. Mechatronics*, vol. 20, no. 2, pp. 684—695, Apr. 2015.

[6] T. Lens and O. von Stryk, "Investigation of safety in human–robot interaction for a series elastic, tendon-driven robot arm," in *Proc. IEEE/RSJ Int. Conf. Intell. Robots Syst.*, 2012, pp. 4309–4314.

[7] B. Bäuml et al., "Agile Justin: An upgraded member of DLR's family of lightweight and torque controlled humanoids," *IEEE Int. Conf. on Robotics and Automation* (ICRA), pp. 2562 – 2563, 2014.

[8] Man Bok Hong and Yung-Ho Jo "Design of a Novel 4-DOF Wrist-Type Surgical Instrument With Enhanced Rigidity and Dexterity," *IEEE/ASME Trans. on Mechatronics*, Vol. 19, Issue. 2, pp. 500 – 511, 2014.

[9] Tomohito Higuma et al., "Low-Profile Two-Degree-of-Freedom Wrist Exoskeleton Device Using Multiple Spring Blades," IEEE Robotics and Automation Letters, Vol. 3, Issue 1, pp. 305 – 311, 2018.

[10] Mark E. Rosheim and Gerald F. Sauter, "New high-angulation omni-directional sensor mount," *Proceedings of Free-Space Laser Communication and Laser Imaging II*, Vol. 4821, pp.163-174, 2002.

[11] Jingjun Yu, Xin Dong, Xu Pei and Xianwen Kong, "Mobility and Singularity Analysis of a Class of Two Degrees of Freedom Rotational Parallel Mechanisms Using a Visual Graphic Approach," *ASME Journal of Mechanisms and Robotics*, Vol.4, 2012.